



Thermal analysis of a high-altitude solar platform

Cristina Beneitez Ortega¹ · Dirk Zimmer¹ · Patrick Weber¹

Received: 28 February 2022 / Revised: 14 November 2022 / Accepted: 19 December 2022 / Published online: 18 January 2023
© The Author(s) 2023

Abstract

High Altitude Long Endurance (HALE) aircraft operate under adverse thermal conditions, with ambient pressures and temperatures very low and at the same time high amounts of heat introduced by sun radiation. Thus, thermal management of the aircraft systems, such as electronics and batteries is a very challenging task. A first step in solving this is generating accurate models of the thermal dynamics of the HALE. This paper presents the thermal analysis of a solar-electric stratospheric HALE at the ground case. A thermal mathematical model based on first principles was developed for such an analysis. In a further step, an initial test campaign was performed. The test campaign included static and dynamic temperature measurements on an aircraft wing structure segment. The experiments throughout this test campaign showed good compliance of the results with the previously derived mathematical models, with differences of less than 5 °C between the measured and simulated temperature curves.

Keywords Thermal management · UAV · HALE · Validation · Green aviation · Space design

1 Introduction

Emerging technologies are shaping the future of aeronautics [1, 2]. Advances in material sciences, power electronics, and energy sources have opened the door to explore potential aircraft alternatives in aerospace [3]. Goals such as greener aviation [4], which a priori seemed distant, are becoming a feasible reality by this technological enhancement. Consequently, unconventional configurations are arising and brought into analysis for their possible implementation in the sector.

HALE aircraft is one example of the new possibilities opened up by enhancing technology. The principle of solar-powered stratospheric flight has been investigated for many

years [5], but only recent advances in battery technology and material science allow implementation with applications for general industrial use. Therefore, the German Aerospace Center's High Altitude Platform (HAP) is planned to be an electrical unmanned aerial vehicle (UAV) operating in the stratosphere, as presented in Fig. 1. Designed as a solar fixed-wing UAV, the propulsion system consists of the interleaved use of energy from solar cells and batteries. This configuration shall allow HAP to serve for satellite like-earth observation and monitoring activities while operating at a cruise altitude of 20 km with a flight endurance of up to 30 days. The adverse environmental conditions in the stratosphere, as well as the innovative UAV configuration HAP will face, are rather extreme for a UAV, enhancing the arising of challenges during the whole design process. In consequence, an exhaustive analysis shall be carried out to ensure HAP successfully completes its mission without endangering its correct operation under these uncommon conditions.

This paper focuses on one of the biggest challenges in the HAP design: thermal management. This uncertainty is addressed by the statement: “How does HAP differ from conventional UAV?”.

To start with, HAP is powered by an electrical propulsion system mainly composed of solar cells and batteries, which power two electric motors with attached constant pitch

Dirk Zimmer and Patrick Weber have contributed equally to this work.

✉ Cristina Beneitez Ortega
cristina.beneitezortega@dlr.de

Dirk Zimmer
dirk.zimmer@dlr.de

Patrick Weber
patrick.weber@dlr.de

¹ Institute of System Dynamics and Control (SR), German Aerospace Center (DLR), Münchener Straße 20, 82234 Weßling, Bayern, Germany



Fig. 1 High altitude platform

propellers. The solar cells are placed on the upper surface of the wing while the batteries are distributed inside the spar of the wing and inside the fuselage. Electric power is generated from the solar-to-electric energy conversion performed by the solar cells during the day and from the batteries during the night [6]. This solar-electric power train architecture, as well as the stratospheric operation scenario including the missions' flight profile, is quite unconventional, no experimental data or literature on the thermal behavior of the solar cells or battery system can be used. Drastic temperature changes in both due to i.e. daytime and nighttime scenarios may take part within each flight phase, affecting their performance and hence the HAP mission.

Aside from the propulsion system, flight altitude at cruise level HAP shall fly is in the stratosphere. In this atmospheric layer, the environmental conditions are critical for electrical devices, i.e. temperatures of $-60\text{ }^{\circ}\text{C}$ can be found at an altitude of 20 km. Heat transfer processes, such as forced convection, become uncertain and very difficult to estimate. In addition, low air density in the stratosphere leads to an unfavorable scenario for the usage of temperature control techniques. While primarily natural convection participates as the most dominant heat transfer process at ground conditions, radiation becomes dominant at high altitudes [7].

Lastly, to achieve an endurance of 30 days, the correct performance of the propulsion system in the described environmental conditions shall be ensured. All the previously described challenges combine during the complete HAP flight profile, leading to the need for an integrated thermal management analysis [8].

The current paper encompasses the description of the extensive thermal analysis developed. As a starting point, Sect. 2 presents the structure of the wing and the equations of the mathematical model which were used to build a detailed numerical thermal simulation of the wing section. In connection, Sect. 3 comprises the tests performed with the section. The segment of the presented wing was equipped with temperature sensors and measurements were carried out. In a further step, a comparison between the numerical model and the experiments was performed, as described in Sect. 4. Lastly, Sect. 5 shows the conclusions drawn from this work as well as the future lines of work.

2 Thermal mathematical model

2.1 HAP wing structure

HAP is classified as a fixed-wing UAV [9]. Defined as a high-wing type, the wing is located at the upper front part of the fuselage. It is characterized by a chord and span of 1.49 m and 12 m respectively when excluding the wingtips. Concerning the layout, from a first design iteration, the surface material is a transparent plastic foil with a thickness of $25 \times 10^{-6}\text{ m}$ which covers the complete wing. Solar cells are located on the wing's upper surface, directly attached to the foil. Regarding the inner structure of the wing, it consists of the main spar, a front spar, and ribs, all of them made of composite material. The ribs are separated from each other by 0.5 m. The spar is a hollow cylinder and has a variable diameter along its length, being the average 0.145 m. Together with the ribs, they form the main skeleton of the structure. Lastly, batteries are placed inside the spar. Following a pattern, the battery blocks are distributed inside the spar with a separation between each other of 0.5 m, being the ribs the reference.

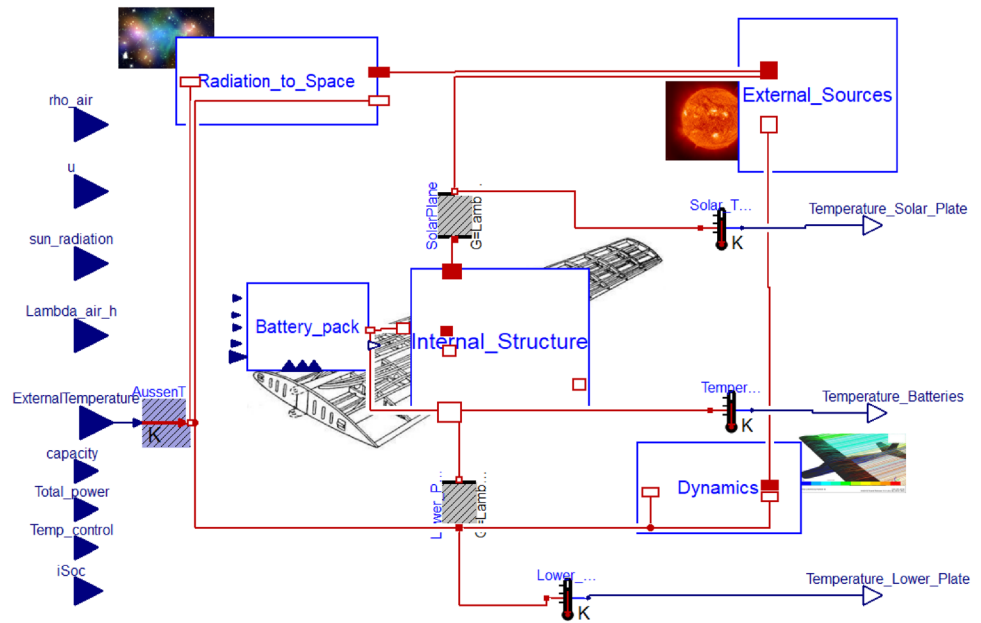
2.2 Model description

The mathematical thermal model is based on thermal interactions in terms of conduction, convection, and radiation. For its development, the Thermal Package of the Modelica Standard Library has been used with Dymola [10] as a simulation tool. The wing structure is defined as the set of heat transfer processes occurring on it. Therefore, all the existing heat sources outside and inside of the wing are first identified.

For the sake of consistency, the model is designed from a collection of Modelica packages. Each package has been established based on the most predominant heat source it contains. The packages are connected following the thermal behavior of the wing. For simplicity purposes, five packages are identified: "Internal Structure", "Battery Pack", "External Sources", "Radiation to Space" and "Dynamics". Figure 2 presents the proposed wing thermal model.

To begin with, the wing's surface is represented by the two conductive parallel plates located in the middle of the model. The upper plate identifies the solar cells meanwhile the lower plate refers to the underside of the wing. Since both plates will face different environmental conditions, radiation and natural convection processes will occur between the two. For completion, the internal structure of the wing is wrapped inside the first thermal package "Internal Structure". Here, the thermal interactions of the

Fig. 2 Wing Modelica model based on first principles



main spar, ribs, and front spar are included. In particular, the thermal conduction of each structural element, as well as the natural convection and radiation processes, occur as a temperature difference between the wing’s surface and each one of the elements. As an extension, the batteries are modeled inside the “Battery pack”. This second package contains a representation of a battery pack that delivers as the main output the natural convection and radiation between the batteries and the wing structure.

Representing the heat transfer processes into mathematical expressions, conduction is defined in the Modelica Standard Library as [11]:

$$Q_{conduction} = kA(T_{1,a} - T_{2,a}) \tag{1}$$

where k is the thermal conductivity of the material, A is the heat transfer area, and $(T_{1,a} - T_{2,a})$ stands for the temperature gradient inside the body a from point 1 to 2.

Similarly, natural convection is represented as:

$$Q_{convection,natural} = hA(T_a - T_f) \tag{2}$$

Being h the convection coefficient, A the heat transfer area, and $(T_a - T_b)$ the temperature difference between a solid a and fluid f taking part in the heat exchange process. By definition, the convection coefficient is dependent on the Grashof number (Gr) and the Prandtl number (Pr) [12]. The convection coefficient is computed as follows:

$$h = \frac{\max(\gamma_{gain}, \gamma_{gain2})\gamma_{air}A}{t} \tag{3}$$

$$\gamma_{gain} = 0.2Gr^{\frac{1}{4}} \tag{4}$$

$$\gamma_{gain2} = 0.073(GrPr^{1.65})^{\frac{1}{3}} \tag{5}$$

The former determines the predominance of the natural convection meanwhile the latter identifies the dominance of the thermal diffusivity,

$$Gr = \frac{t^3 g \beta (T_a - T_b)}{\nu} \tag{6}$$

$$Pr = \frac{\mu c_p}{\gamma_{air}} \tag{7}$$

where γ_{air} represents the thermal conductance of air at a specified altitude, t the distance between each body, g the gravity, β the coefficient of thermal expansion, ν the kinematic viscosity, c_p is the specific heat of the air and, μ the dynamic viscosity at a specified altitude, estimated with the Sutherlands approximation [13]:

$$\mu = \mu_s \left(\frac{T}{T_s}\right)^{\frac{3}{2}} \left(\frac{T_s + 110.4}{T + 110.4}\right) \tag{8}$$

being μ_s the reference dynamic viscosity and T_s the reference temperature of $1.716 \cdot 10^{-5}$ kg/ms and 273.15 K, respectively.

Lastly, radiation occurring inside the HAP wing structure is described as:

$$Q_{radiation,2bodies} = A\sigma F\epsilon(T_a^4 - T_b^4) \tag{9}$$

σ represents the Boltzmann constant, F defines the area of view between the two bodies and ϵ is the emissivity factor of the surface of the body. Since each body may have a different emissivity factor (i.e. transparent foil and composite material), the value is then described by a combination of them:

$$\epsilon = \frac{\epsilon_a \epsilon_b}{\epsilon_a + \epsilon_b - \epsilon_a \epsilon_b} \tag{10}$$

Focusing on the environmental conditions, three more packages are defined. An important remark to point out is the invalidity of the International Standard Atmosphere (ISA) model for altitudes higher than 15 km. [14] Hence, treating air as an ideal gas and assuming a known behavior, NRLM-SISE-00 Atmospheric Model from NASA is utilized [15]. The model is valid for altitudes higher than 12 km.

The third package is “External Sources”. It contains the heat flow contributions from the environment to the wing. Sun radiation, albedo radiation, and planetary radiation are the principal heat sources included. Meanwhile the former is directly acting on the solar cells, and the latter two have an impact on the temperature on the underside of the wing [16].

$$Q_{radiation,sun} = A\alpha S_s \tag{11}$$

$$Q_{radiation,albedo} = A\alpha a S_s \tag{12}$$

$$Q_{radiation,planetary} = 237A\alpha \left(\frac{RE}{RE + h} \right)^2 \tag{13}$$

where α stands for the absorptivity factor of the material, S_s for the solar radiation, RE for the radius of the Earth, and h the altitude with respect to the Earth’s surface. As for the albedo radiation, it is directly proportional to the sun radiation: $S_a = F S_s$, being a the albedo coefficient the Earth’s surface has. For this analysis, a fixed value of 0.3 is defined [16].

In the same line of thought, the “Radiation to Space” package represents the radiation emitted from the wing to the environment as a result of the heat processes acting on it. Due to the difference in the material on the wing, both upper and lower surfaces are treated separately. Here, T_{amb} represents the ambient temperature at each altitude.

$$Q_{radiation,environment} = A\sigma\epsilon(T_a^4 - T_{amb}^4) \tag{14}$$

The motion of the HAP in the environment leads the air to flow along the surface of the wing. In consequence, forced convection occurs, as shown in the “Dynamics” package. The airfoil shape and the settling of the material on both wing surfaces generate a different local flow velocity, which makes it necessary to include two different forced convection processes. From preliminary calculations based on the Reynolds number, the flow has been defined to be turbulent

at the upper part of the wing and laminar at the underside. Its local velocity has been assumed to be 1.3 times the aircraft velocity on the upper side and 0.9 on its underside.

$$Q_{convection,forced} = wNu\lambda_{air} \tag{15}$$

w is the characteristic length (i.e. span), Nu is the Nusselt number governed by the airflow regime [17] and λ_{air} is the air conductivity:

- For laminar flow:

$$Nu = 0.664Re^{\frac{1}{2}}Pr^{\frac{1}{3}} \tag{16}$$

- For turbulent flow:

$$Nu = 0.037Re^{\frac{4}{5}}Pr^{\frac{1}{3}} \tag{17}$$

with Re as Reynolds number dependent on the air velocity u and the characteristic length L , being, in this case, the wing chord:

$$Re = \frac{u\rho L}{\mu} \tag{18}$$

Lastly, to represent the dynamic behavior, the heat capacity C shall be implemented. By definition, the amount of energy that must be added to an object to raise its temperature by one degree is known as heat capacity [18]. C depends on the specific heat of the material c_p and its mass m . For the analysis, the heat capacity of each material of the structure was identified.

$$C = c_p m \tag{19}$$

Concluding with the overview, the wing thermal model is a combination of five Modelica packages, connected as represented in Fig. 3. Nine inputs are introduced into the model, which can be identified in two groups. First, the model requires as input the atmospheric conditions at each altitude of the flight profile. Accordingly, air thermal conductivity, temperature, density, velocity, and solar radiation are the five inputs defined for the purpose described. Furthermore, the battery pack requires additional parameters and state variables for its operation. For this purpose, four additional inputs are defined: battery capacity, battery power, battery state of charge (SOC); and an extra input to control the heating energy needed by the battery under low-temperature conditions. As outputs, the model provides an estimation of the temperatures at each surface of the wing as well as the magnitude of the heat emitted and delivered. However, in this paper, we will just focus on the temperature of the solar cells, the temperature of the batteries, and the temperature at the underside of the wing as outputs.

2.3 Model inputs

The HAP flight profile shall comprise altitudes from sea level to 25 km, with a cruising altitude of 20 km. Due to the uncertainty of the location on Earth HAP will fly, the two geographic latitudes with the most extreme thermal conditions have been set for the analysis: Kiruna (67 ° N)

and close to Italy (35 ° N). As the season has also an influence (length of daylight, incidence angle of the sun) only the better case (summer) is selected. Tables 1 and 2 show the atmospheric conditions as inputs utilized for each scenario using the NRLMSISE-00 atmospheric model [15].

With respect to the inputs for the battery block, the capacity of each battery pack has been defined at a value

Fig. 3 Heat transfer processes in the wing section

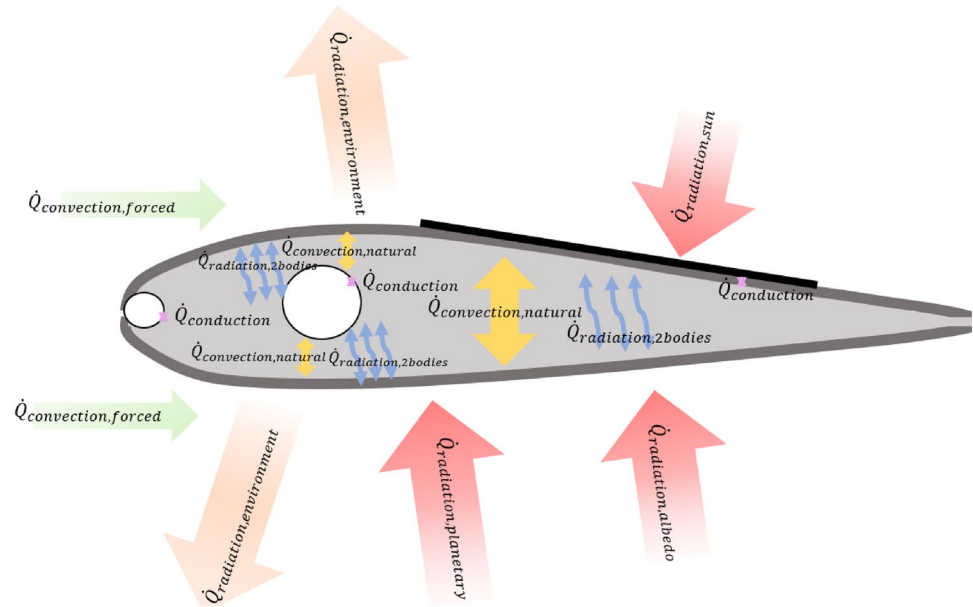


Table 1 Atmospheric conditions—Italy

Altitude (km)	Sun radiation (W/m ²)		Temperature (°C)	Density (kg/m ³)	Speed (m/s)	Air thermal conductivity (W/mK)
	DAY	NIGHT				
0	896	0	22	1.204	9	0.02601
5	1106	0	-5	0.724	11.5	0.02396
10	1211	0	-40	0.423	15.5	0.02121
15	1266	0	-64	0.217	22.1	0.01925
20	1294	0	-60	0.09465	31	0.01958
25	1308	0	-50	0.0416	41.8	0.0204

Table 2 Atmospheric conditions—Kiruna

Altitude (km)	Sun radiation (W/m ²)		Temperature (°C)	Density (kg/m ³)	Speed (m/s)	Air thermal conductivity (W/mK)
	DAY	NIGHT				
0	832	29	4	1.274	9	0.02465
5	1058	0	-21	0.737	11.5	0.02272
10	1181	492	-45	0.397	15.5	0.0208
15	1249	743	-46	0.187	22.1	0.02072
20	1284	942	-44	0.0886	31	0.02088
25	1302	1082	-41	0.0417	41.8	0.02113

of 433Wh. As previously stated, the solar cells shall be the source of electric power during the daytime and the batteries in the nighttime. As an additional remark, the solar cells shall be able to power HAP as well as charge the batteries during the daytime case. Hence, the power balance during the day is defined as:

$$P_{solar} = P_{propulsion} + P_{charge} \tag{20}$$

being $P_{propulsion}$ the electric power for propulsion and P_{charge} the electric power for charging the batteries.

To sum up, the power entering into the battery block when used (“batteries on”) and when not (“batteries off”) is defined in Table 3. All the simulations have been performed with the batteries discharging and reaching a minimum SOC of 0.3.

2.4 Model results: temperature distribution across the wing

Figure 4 depicts the temperature distribution in the wing structure and the batteries for both day and night cases in Italy. For this analysis, it has been assumed a homogeneous surface temperature along the wing. For the wing structure

characterization, three reference points are identified: the solar cells, the underside of the wing, and the compartment. Similarly, the battery block is represented by the internal temperature.

As shown in Fig. 4, the wing temperature from the cross-sectional perspective is defined by temperature distribution with its maximum at the solar cells and its minimum at the underside of the wing. Additionally, the highest temperatures are achieved at ground level meanwhile the lowest are found at 15 km altitude. Above 15 km, temperature values in the stratosphere increase again, leading to an increment in the temperature distribution in the wing. Focusing on the solar cells, temperatures within the range of -10°C to 40°C during the day and -45°C to 20°C during the night case are found. About the batteries, they reach values from -15°C to 40°C during the daytime and values from -15°C to 28°C during the night, opening the door to the design of temperature control techniques [19]. These values are estimated from the battery’s performance. However, using the batteries during the day and having them off during the night will lead to a different temperature distribution concerning altitude. All combinations shall be studied in further analysis.

Similarly, Fig. 5 illustrates the temperature distribution in the wing for the day and night case at Kiruna. Due to the existing environmental conditions at this location (see Tables 1 and 2), the temperatures at each reference point of the wing differ significantly from the Italy case. As an example, nighttime in Kiruna is governed by high and constant solar radiation as altitude increases. Thus, different temperature outputs are expected. Regarding the solar cells, a minimum temperature of -5°C and a maximum of 50°C during the day are observed. For the night case, values drop between -25°C and 35°C . The complete wing structure is subjected to night temperatures in the range of 0 to -30°C . Concerning the battery blocks, they reach values from -10°C to 35°C during the daytime and values from -5°C to 40°C during the night.

Table 3 Power entering in the batteries

Altitude (km)	Power per block “Batteries on” (W)	Power per block “Batteries off” (W)
0	28	0
5	73	0
10	98	0
15	113	0
20	113	0
25	113	0

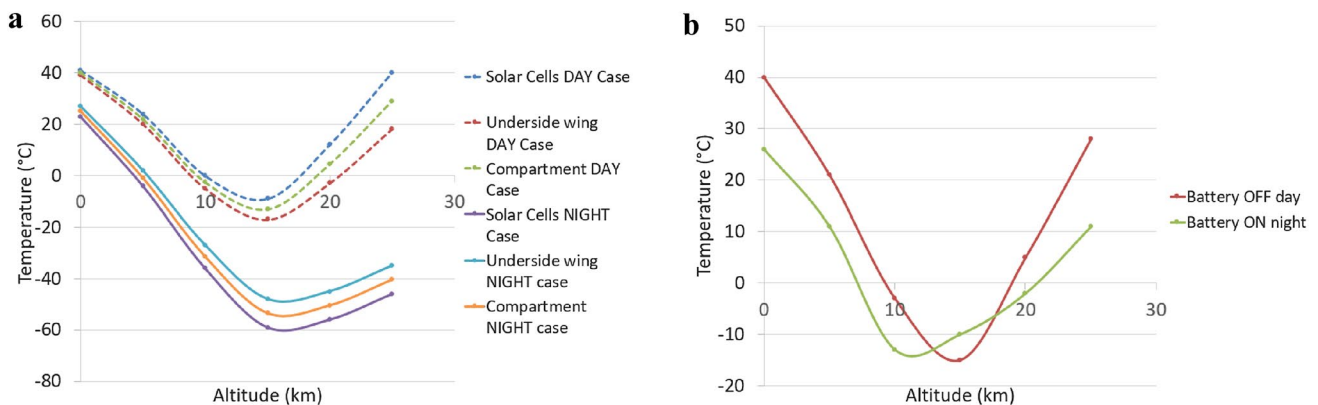


Fig. 4 a Temperature distribution inside the wing structure. b Temperature distribution at the battery block—Italy scenario

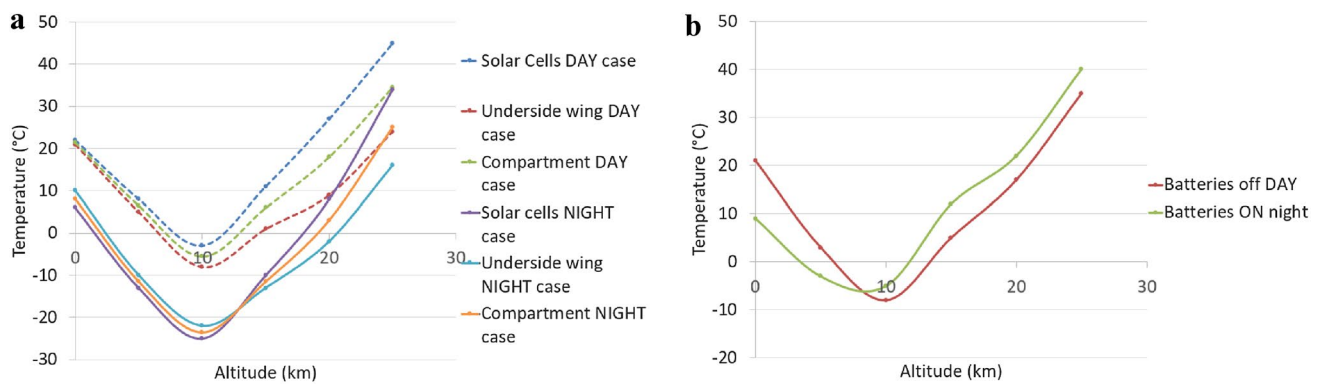


Fig. 5 **a** Temperature distribution inside the wing structure. **b** Temperature distribution at the battery block—Kiruna scenario

To sum up, the presented model, based on the first principles, allows us to study the thermal interactions occurring inside the HAP wing. The temperature results obtained are considered preliminary and shall be subjected to validation activities.

3 Experimental approach

3.1 Introduction

The objective pursued in the present work is to estimate the temperature distribution inside the HAP wing section. Thus, to determine the consistency and reliability of the wing Modelica model, tests shall be performed.

For simplicity purposes, the first test at ground conditions was carried out. The experiment aims to estimate the heat transfer processes occurring in the wing, as well as the temperature distribution across it for two test variants: dynamic and stationary. For the dynamic case, the wing was mounted on the roof of a car and driven on a runway until the steady state was reached. As for the stationary case, the wing was positioned still on the taxiway.

3.2 Setup

For the realization of the experiment, a section of the central part of the wing was utilized. The section was a replica of the real wing but with a length of 3 ms. Keeping its configuration, the wing surface was made of plastic transparent foil, with dummy solar cells located on the top of the wing upperside surface. The internal structure consisted of the main spar, a front spar, and a set of ribs, depicted in Fig. 6. For reasons of cost efficiency, no real solar cells were used but solar dummies, consisting of black tape attached to a copper laminate. Inside the section, the front and main spar and the ribs were placed. Batteries have not been included in this test variant, since it is desired, as a first step, to estimate the temperature in the compartment where they will be placed. Further validation activities shall be carried out for detailed validation of the surface temperature of the batteries. In addition, the wing had a mounting system made of wood for easier placement at the roof of the car, as shown in Fig. 7.

To measure the temperatures, temperature sensors were incorporated inside the wing. For this analysis, three locations were selected: solar dummies, the underside of the

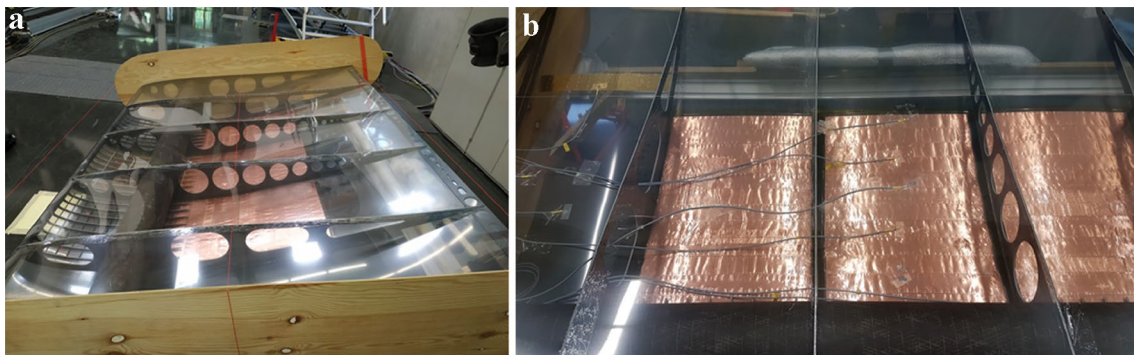


Fig. 6 **a** Wing section for the tests—upside down. **b** Temperature sensors at the solar dummies and underside of the wing



Fig. 7 Set up and anemometer placement

wing, and the spar. Since there were no batteries inside the section, sensors were situated at the spar to estimate the temperature the batteries shall face. Additionally, the roof of the car also incorporated sensors on the chassis. To keep redundancy as well as avoid the loss of data, a pair of sensors was placed at each location. Sensors were calibrated before the test realization.

Solar radiation was evaluated using two lux meters. As a similar approach, two lux meters (on the ground and on the car) were utilized for redundancy and calibration purposes. The estimation of the ambient temperature was obtained by a thermometer. Lastly, an anemometer was included on the wing structure, providing true airspeed.

3.3 Dynamic experiment—results and post-processing

As the first variant in the test campaign, dynamic tests were carried out. The test aimed to reproduce the wing thermal behavior as in HAP. The wing, mounted on the roof of the car, was driven along the runway at different times of the day, being the solar radiation, airspeed, and ambient temperature the main variables measured during the testing. The duration of each test depended on the time needed to reach a steady state, with an average of 20 min for the desired locations to be tested. The test campaign lasted from 18th to 20th August 2020, however, the present section contains one of the tests with the most promising results.

The boundary conditions for the experiments were based on the HAP flying conditions at the ground level presented in Table 1. Making use of the anemometer, the true airspeed for each test was set. For each experiment, a speed between 6 to 15 m/s was sought. The results analyzed in this section represent the case of an average speed of 6.5 m/s. Regarding the atmospheric conditions, solar radiation and an ambient temperature of 580 W/m² and 25.5°C were found, respectively. The test was performed at DLR Oberpfaffenhofen, with its geodetic latitude and altitude above Mean Sea Level

(MSL) defining the remaining environmental conditions as air density and air pressure of 1.203 kg/m³ and 1014 hPa, respectively [20].

From the temperature outputs, it can be concluded that after 20 min, the steady state was reached. As shown in Fig. 8 for the solar dummies, the temperature mostly oscillated between 45°C and 50°C meanwhile the temperature at the underside of the wing illustrated in Fig. 9 varied from 36°C to 38°C. Concerning the spar surface, it was warmed up to 44°C to 47°C. Focusing on the temperature distribution, higher oscillations are found on the wing surface (solar cells and wing underside) than at the spar. A possible cause could be the effect of the wind on both surfaces. Also, the 180° turns, with a reduction of the speed for a short moment, were required on the runway, leading to a different incidence of the sun and airflow on the wing structure. The amount of solar radiation absorbed by the wing section also influences the thermal distribution. As shown in Fig. 9b, clouds covered the sun at some intervals, such as at 2.5 and 11 min, leading to a decrease in the amount of absorbed radiation, reflected in Fig. 9a. In addition, the heat capacity of each material is different, impacting its temperature distribution.

3.4 Stationary experiment—results and post-processing

The purpose of the stationary test relies on the estimation of the temperatures at the wing structure when there is no wind speed hence forced convection does not take place. For such analysis, the car was parked at the runway and the temperatures were measured until the equilibrium point was reached. During the test, an average value of the true airspeed of 0.14 m/s was measured. The solar radiation and ambient temperature had an average value of 580 W/m² and 28°C, respectively.

The temperature outputs are shown in Figs. 10 and 11. For the first 5 min, the car was stored inside the hangar and placed later on the runway. Regarding the temperature

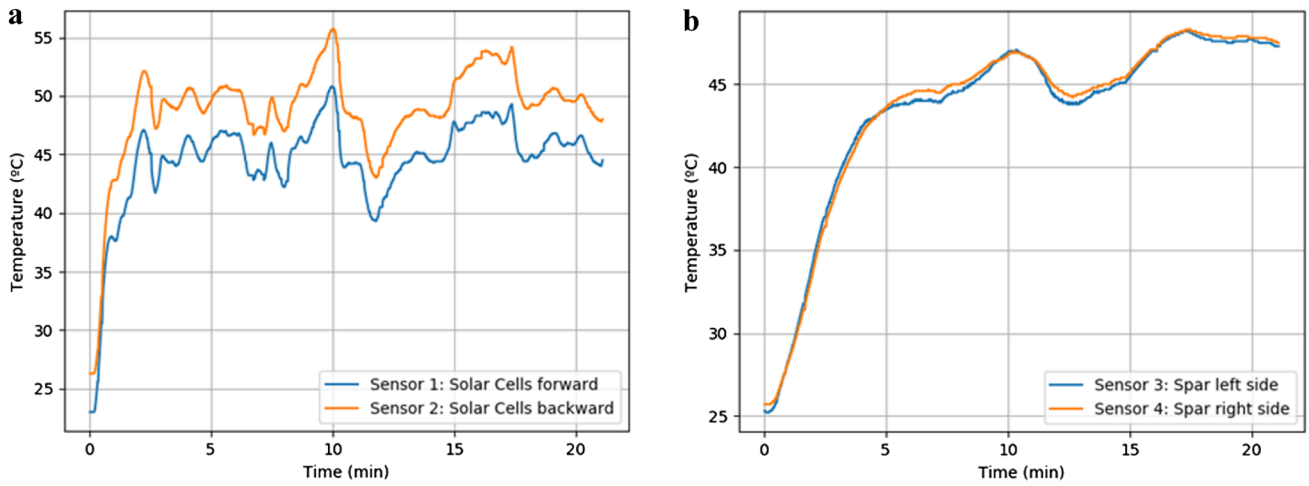


Fig. 8 a Temperature output solar dummies. b Temperature output spar

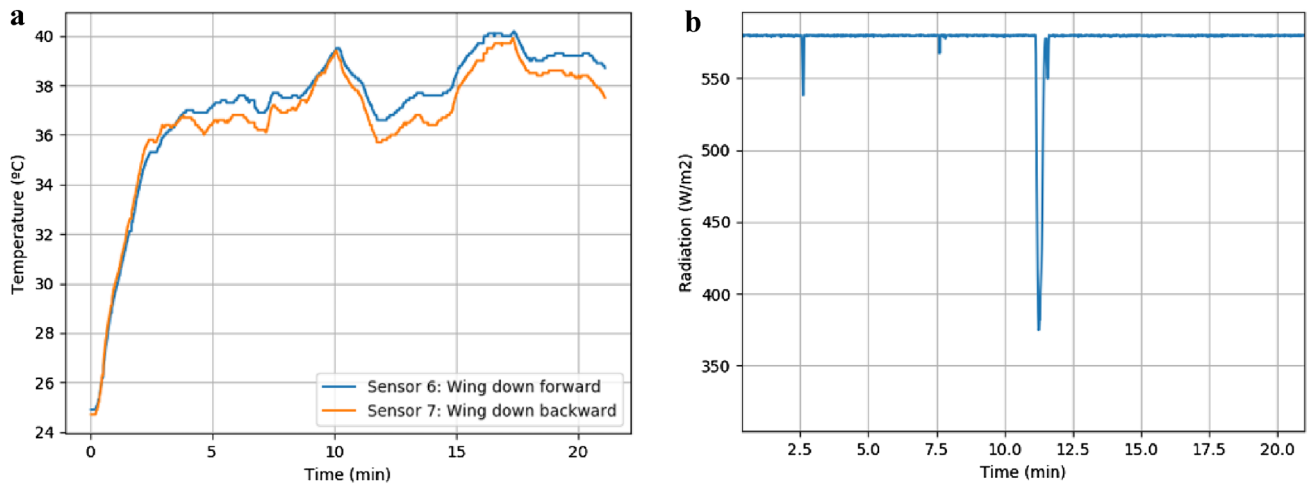


Fig. 9 a Temperature output underside wing. b Radiation marked by the luxmeter

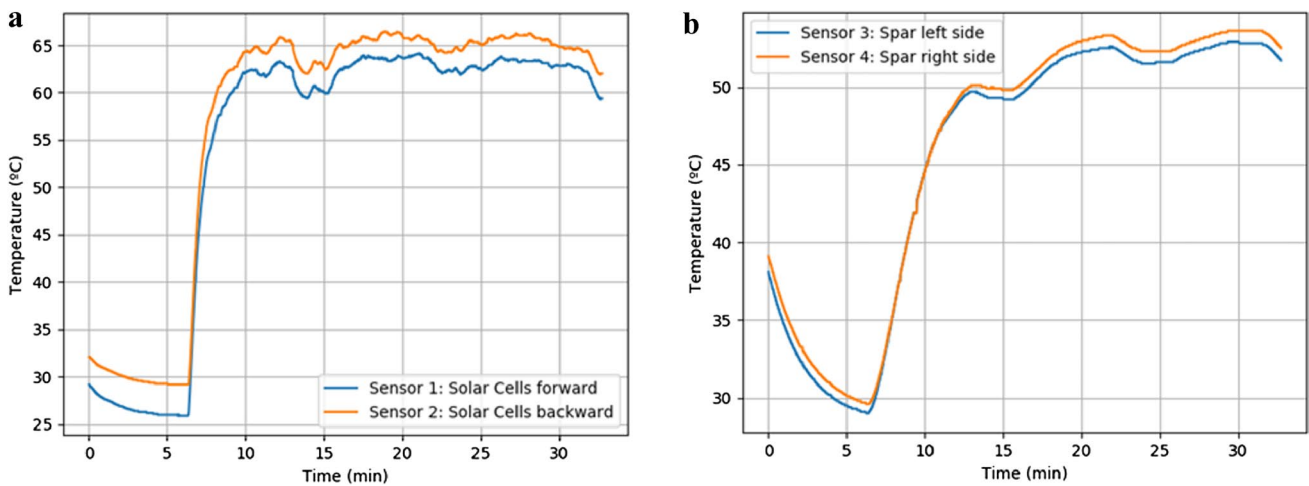


Fig. 10 a Temperature output solar dummies. b Temperature output spar

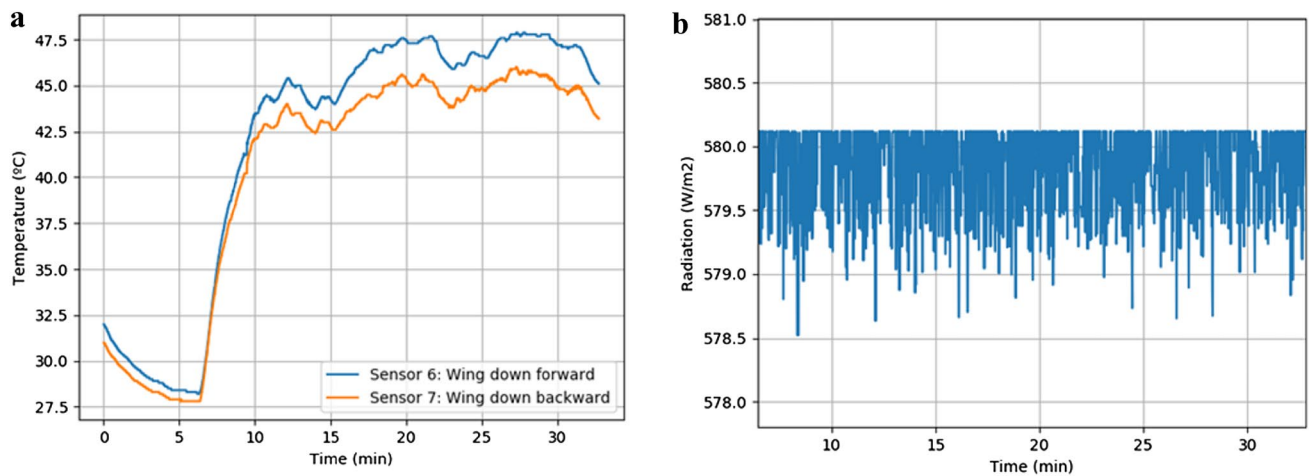


Fig. 11 **a** Temperature output underside wing. **b** Radiation marked by the luxmeter

distribution, the solar cells were warmed up to 62°C to 64°C. Here, smaller oscillations in the values are shown, which strengthens the presumption they are caused by the wind effect and the heat capacity of the material. The analysis proves the high impact forced convection has on the structure, especially at low speeds. These oscillations can also be seen on the underside of the wing, where its value has also decreased for the dynamic test. Finally, the surface temperature at the spar varied from 53°C to 54°C.

4 Thermal mathematical model validation

Temperature measurements from the test campaign were utilized for the validation of the Modelica model. First off, the numerical model was adapted to the conditions that describe the tests. All the heat transfer processes occurring during the experiments must be outlined in the Modelica model. To start with, both albedo and planetary radiation contributions were neglected in the analysis, since none contribute to ground conditions. The transparent foil on the top of the wing created a greenhouse effect between the sun and the inside of the wing, thus adding another contribution of sun radiation. In addition, the thermal contribution of the car roof to the wing section was included. Radiation, natural convection, and forced convection occurred between the car roof and the wing surface. In the stationary case, the absence of wind and, therefore, the lack of forced convection, identifies natural convection and radiation as the most dominant heat transfer processes. Furthermore, the heat capacity of each material was also added in the Modelica model.

As inputs, the model was defined by: the solar radiation measured by the luxmeter, the ambient temperature recorded by the thermometer, and the true airspeed measured by the anemometer, as depicted in Fig. 12.

The density and the thermal conductivity of the air were set as a function of the temperature and altitude at which the experiments were conducted. In the interest of completeness, the tests were conducted at DLR Oberpfaffenhofen.

4.1 Model validation for the dynamic variant

The dynamic variant was recreated using Dymola as a simulation tool. Figure 13 compares the temperature distribution at the wing obtained from the Modelica model and from the test. For improved visualization, a low-pass filter has been implemented. The comparison shows a temperature offset at each location between the two approaches of approximately 3°C.

The temperature distributions in both approaches, defined mainly by the heat capacity of the materials, are very similarly identified. Thus, although it can be concluded the Modelica model was partially validated, there are still unresolved uncertainties. As an example, the largest temperature difference can be seen at the spar, whose value in the experimental approach was around that of the solar dummies. Numerous are the effects that can affect this temperature value, such as the combination between the heat capacity of the materials and the forced convection between the solar dummies and the air. Therefore, further validation tests shall be performed for the validation of the Modelica model.

4.2 Model validation for the stationary variant

Similarly, Fig. 14 comprises the temperature outputs of the numerical simulation and the experiment. Between the thermal distributions obtained from both, a maximum offset of 2°C is depicted in the figure. As a consequence of a stationary test, smaller oscillations are seen in the thermal behavior of the material. Again, the largest temperature offset is found

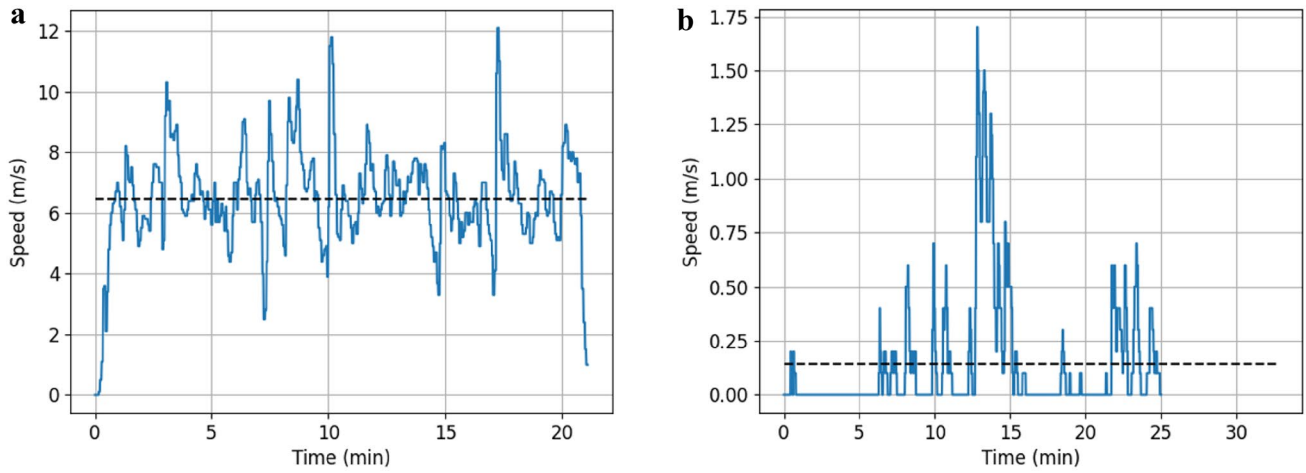


Fig. 12 a Airspeed—Dynamic case. b Airspeed—Stationary case

Fig. 13 Numerical and experimental comparison—dynamic experiment

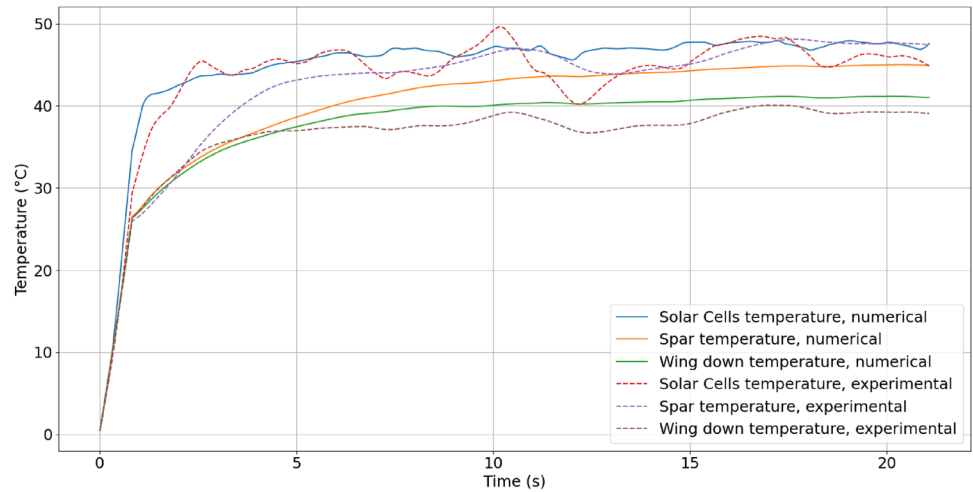
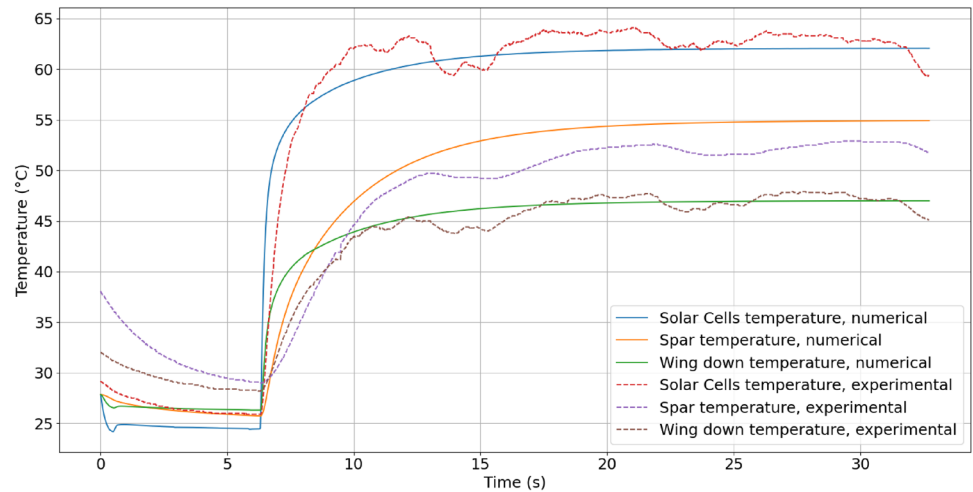


Fig. 14 Numerical and experimental comparison—stationary experiment



at the spar, which confirms, among others, the high impact of forced convection at low speeds and its relation with the thermal distribution across the wing structure.

5 Conclusions and future work

In this paper, the thermal analysis of the HAP wing structure was presented. The analysis was performed with an analytical model based on the first principles for conduction, convection, and radiation phenomena. As outputs, the model provided estimations of the temperature distribution across the wing, with the main reference points being the solar cells, spar, and the lower part of the wing. To estimate its accuracy, experiments were carried out. A section of the wing was utilized to perform both dynamic and stationary tests. In post-processing, the previously introduced simulation model was fed with the experimental conditions and the simulation results have been compared to the experimental measurements. The results showed a maximum temperature offset between both approaches of 5 °C for the dynamic case and 2 °C for the static test. They have been considered to be the best case scenario taking into account the possible uncertainties that occurred during the experiments. To reduce the current offset, further testing is planned. Improvements will be based on i.e. the use of real solar panels and the inclusion of the batteries inside the spar. Afterward, tests will be carried out to validate the mathematical model at higher altitudes.

Thermal management of the HAP does not include only the wing but encompasses the entire HAP structure. Hence, a thermal analysis shall be performed to estimate the temperature the remaining structure and the equipment will face throughout the mission and define temperature control techniques to keep them within their operating temperature range.

Acknowledgements The presented work has been internally funded by the German Aerospace Center. The authors wish to thank DLR Braunschweig for providing the wing section and the equipment necessary for the model validation; in particular Andreas Bierig, HAP project leader, together with Patrick Gallun. Further thanks go to Gertjan Looye, Daniel Milz, and Oberpfaffenhofen airport for their support during the tests. In addition, we like to thank Christian Weiser for his continuous feedback and his valuable insights on the subject.

Funding Open Access funding enabled and organized by Projekt DEAL.

Open Access This article is licensed under a Creative Commons Attribution 4.0 International License, which permits use, sharing, adaptation, distribution and reproduction in any medium or format, as long as you give appropriate credit to the original author(s) and the source, provide a link to the Creative Commons licence, and indicate if changes were made. The images or other third party material in this article are included in the article's Creative Commons licence, unless indicated

otherwise in a credit line to the material. If material is not included in the article's Creative Commons licence and your intended use is not permitted by statutory regulation or exceeds the permitted use, you will need to obtain permission directly from the copyright holder. To view a copy of this licence, visit <http://creativecommons.org/licenses/by/4.0/>.

References

1. International Air Transport Association (IATA). Technology Roadmap, 4th Edition (2013)
2. Mbarki, S., Marulo, F.: The Innovation of Electric and Hybrid Aircraft, Tesi di Laurea, Università degli Studi di Napoli "Federico II", 2019-2020
3. Bargsten, C.J., Gibson, M.T.: NASA Innovation in Aeronautics: Select Technologies That Have Shaped Modern Aviation, *NASA/TM-2011-216987* (2011)
4. DLR. Zero Emission Aviation, German Aviation Research White Paper (2019)
5. Noll, T.E., Brown, J.M., Perez-Davis, M.E., Stephen, I.D., Tiffany, G.C., Gaier, M.: Investigation of the Helios Prototype Aircraft Mishap, Volume 1 (2004)
6. Noth, A., Siegwart, R., Engel, W.L.: Design of Solar Powered Airplanes for Continuous Flight (2006)
7. Mei, K., Xueyin, S., Yuanzhu, P., Cheng, L., Xinying, K., Jingjing, D., Zhegui, H.: Thermal design and optimization of the stratospheric airship equipment module. *J. Phys. Conf. Ser.* (2020)
8. Airbus Defence and Space: Zephyr. Press release, Zephyr S set to break aircraft world endurance record (2018)
9. Nikodem, F., Biereig, A.: DLR: HAP - Herausforderungen in der Entwicklung der DLR Höhenplattform und ihrer Anwendungen (2020)
10. Dymola: Dynamic Modeling Laboratory, Dymola Release Notes (2020)
11. Shapiro, H.N., Moran, M.J.: Boettner D D, 8th edn. Bailey M B, Fundamentals of Engineering Thermodynamics (2014)
12. Mayinger, S.: Thermodynamik p. 459 (2007)
13. Sutherland, W.L.: The viscosity of gases and molecular force. *Philosophical Magazine Series 5* (1893)
14. Picone, J.M., Hedin, A.E., Drob, D.P., Aikin, A.C.: NRLM-SISE-00 empirical model of the atmosphere: Statistical comparisons and scientific issues. (2002)
15. Evrim, Briese, L., Klöckner, A., Reiner, M.: The DLR environment library for multi-disciplinary aerospace applications. International Modelica Conference (2017)
16. Merino, M.: Thermal Control - Space Systems Design for MSC Aeronautical Engineering master class. University lecture, 2017–2018
17. Bahrami, M.: Forced Convection Heat Transfer, Master class (2011)
18. Bhandari, S.: Chapter 6: Specific Heat, Latent Heat, and Heat Capacity Goals of Period 6 (2012)
19. Ma, S., Jianf, M., Tao, P., Song, C., Jianbo, W., Wang, J., Deng, T., Shang, W.: Temperature effect and thermal impact on lithium-ion batteries: a review. *Progress Nat. Sci. Mater. Int.* **28**(6), 653–666 (2018)
20. EDMO METAR - Oberpfaffenhofen airport database, 2020

Publisher's Note Springer Nature remains neutral with regard to jurisdictional claims in published maps and institutional affiliations.